Supplementary Information for **Superconductivity in the infinite-layer nickelate superlattice**

Wen Xiao[1], Zhan Yang[1,2], Shilin Hu[1], Yuzhou He[3], Xiaofei Gao[1], Junhua Liu[1], Zhixiong Deng[1], Yuhao Hong[1], Long Wei[1], Lei Wang[1], Ziyue Shen[1], Tianyang Wang[1], Lin Li[1], Yulin Gan[1]*, Kai Chen[1]*, Qinghua Zhang[3]*, Zhaoliang Liao[1]*

[1]*National Synchrotron Radiation Laboratory, School of Nuclear Science and Technology, University of Science and Technology of China, Hefei, 230029, China*

[2]*School of Physics, Zhengzhou University, Zhengzhou 450001, China*

[3]*Beijing National Laboratory for Condensed Matter Physics, Institute of Physics, Chinese Academy of Sciences, Beijing 100190, China*

*To whom correspondence should be addressed. E-mail: zliao@ustc.edu.cn, zqh@iphy.ac.cn, kaichen2021@ustc.edu.cn, ylgan@ustc.edu.cn

Note1: Critical thickness in reduced nickelate SLs

Firstly, $[(Nd_{0.8}Sr_{0.2}NiO_3)_n/(SrTiO_3)_3]_{10}$ (note as N_n/S_3) superlattices (SLs) with varying nickelate thicknesses were grown by pulsed laser deposition (PLD) monitored in-situ by reflected high-energy electron diffractometer (RHEED). The number of unit cells in the $Nd_{0.8}Sr_{0.2}NiO_3$ and $SrTiO_3$ layers was controlled by observing intensity oscillations of diffraction spots (Figure S1). The condition of the as-grown SLs evolved with the nickelate thickness, as depicted in Figure S2. With the increasing of nickelate thickness, the surface gradually developed particles, leading to an increase of surface roughness (Figure S2b). Since nickel was enriched on the target surface during pulsed laser deposition of nickelate targets, leading to the formation of a number of non-chemically stoichiometric NiO_x particles on the film surface during the continuous growth process, which was dependent on the deposition time[1,2]. Despite the presence of these particles, all SLs samples exhibited very high quality with superlattice satellite peaks and continuous Laue oscillations (Figure S2a).

Figure S3(a) and (b) shows XRD θ-2θ symmetric scans of as-grown $[(Nd_{0.8}Sr_{0.2}NiO_3)_n/(SrTiO_3)_3]_{10}$ (note as N_n/S_3) and $[(Nd_{0.8}Sr_{0.2}NiO_2)_n/(SrTiO_3)_3]_{10}$ (note as R-N_n/S_3) after topotactic reduction. It can be seen that the structure of R-N_n/S_3 is depended on the thickness of nickelates (n). While n is less than 5, the reduced SLs main (00l) peak essentially unchanged, revealing that the crystal structures of these SLs are not planar infinite layer structure. Nevertheless, as n is larger, the (00l) peak moves towards the peak corresponding to infinite-layer, demonstrating a transition towards infinite-layers. In general, the lattice constant of a SL can be calculated by $c_{SL} = (n * c_A + m * c_B)/(n + m)$, where c_{SL}, c_A, c_B, n , m are lattice constant of SL, materials A layers, material B layers and the corresponding unit cell number, respectively. Figure S3c shows the summarized statistics for the c-axis lattice constant of N_n/S_3 (black line) and R-N_n/S_3 (red line), and the theoretical values calculated by the above formula using the infinite-layer nickelate lattice constant [$c(Nd_{0.8}SrNiO_2)$ = 3.37 Å] are marked with a blue line. Compared to the theoretical value, there is a sudden decrease while n is between 4 and 5, which is consistent with the phenomenon observed in the $SrCuO_2$ SLs[3-6]. The drastic change of c value is also evident in the reciprocal space mapping (RSM) as shown in Figure S4.

In order to exclude the effect of inadequate reduction, the variation of superlattice XRD peak positions with reduction time was investigated (Figure S5). It can be observed intuitively that the main peak position of the N_9/S_3 superlattice shifted little after 10 h of calcium hydride reduction, then underwent a significant change and reached saturation after 8 hours of continuous reduction, and finally remained essentially unchanged even after an additional 2 hours of reduction. Conversely, the XRD patterns of the N_3/S_3 superlattice showed minimal change after 20 hours of reduction. The trends in c-axis lattice constants of different superlattices over reduction time are depicted in Figure S5b. As the thickness of the nickelate layer in SLs increases, the time required for complete reduction also increases. Under identical conditions, the thicker nickelate layer will require more time to be fully reduced. All SLs can be completely reduced after 20 hours.

X-ray reflectivity (XRR) was employed to analyze the thickness of SLs (Figure S6). The thickness of the N_3/S_3 SL remained constant after reduction, with the X-ray SLD profile from XRR showing consistent amplitude and phase, in contrast to the measurements of N_9/S_3, which exhibited variation. These results provide further evidences of a critical thickness threshold for structural changes in nickelate SLs.

In summary, the thickness of the nickelate layers (*n*) significantly influences the structure of the reduced superlattices. While *n* is less than 4, as-reduced SLs are difficult to lose oxygen during reduction, presenting the similar XRD pattern with as-grown SLs. With the increasing of *n*, SL_S tend to lose apical oxygen and turns to infinite-layer structure. Nevertheless, the structure of R-N_5/S_3, RN_7/S_3 and R-N_9/S_3 did not convert to a pure infinite-layer even through completely reduce. The results of the lattice constants calculated by XRD show that the actual lattice constants deviate from those calculated using the theoretical values of the infinite-layer nickelates. It suggests that the nickelate obtained here may have some Ruddlesden–Popper (RP) phase, leading to the inability to obtain a superlattice with a pure infinite-layer structure. It has been reported that RP phase $RE_4Ni_3O_{10}$ (*RE* means Rare Earth Element) shows the similar XRD (00*l*) peak as perovskite $RENiO_3$[7-9]. We notice that the nickel enrichment of stoichiometrically doped nickelate targets during pulsed laser deposition tends to predispose to the formation of such defective RP phases during film growth[1]. Therefore, the Nd/Ni stoichiometry ratio is particularly important during pulsed laser deposition[10,11]. In order to counteract the effect of nickel enrichment during deposition on the obtained thin film phase, we increased the ratio of nickel in the target used for deposition, resulting in a Nd/Ni ratio of 1.15 in the target[12,13].Then we used the same growth parameters to regain the nickelate superlattice and reduced to obtain superconducting infinite-layer superlattice films, the relevant discussion is in the main text.

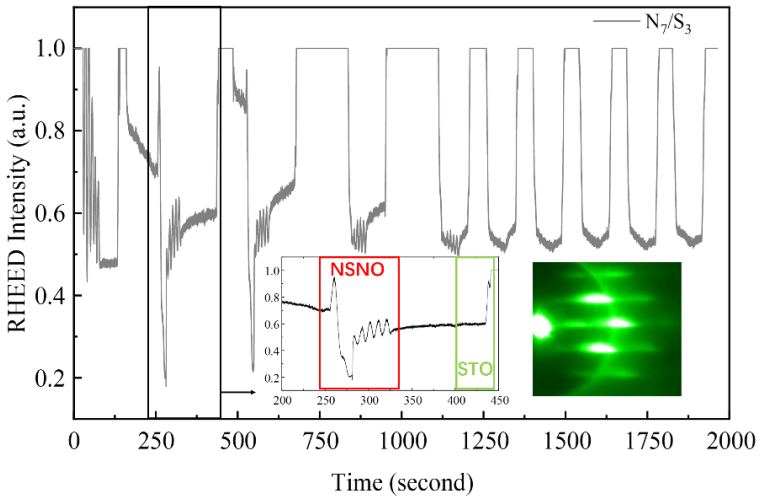

Figure S1. In situ monitoring of $(N_7/S_3)_{10}$ superlattices layer-by-layer growth through reflective high-energy electron diffraction intensity, each oscillation of intensity represents the growth of an atomic layer. Inset: Zoom-in view of the oscillation per cycle and RHEED pattern after growth.

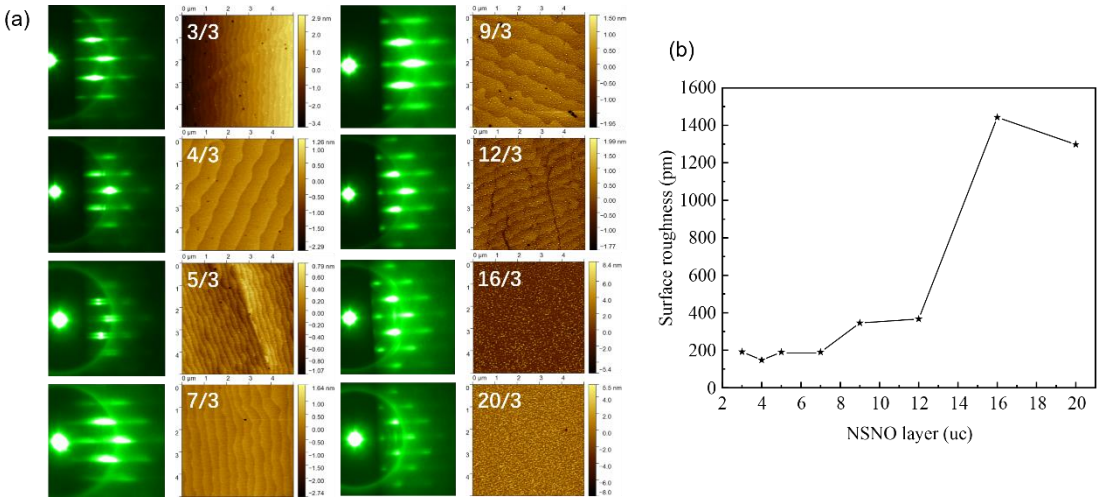

Figure S2. **(a)** Reflective high-energy electron diffraction(RHEED) images and surface morphology characterized by atomic force microscopy (AFM) of various $(N_n/S_3)_{10}$ superlattices surfaces. **(b)** Surface roughness of various superlattices.

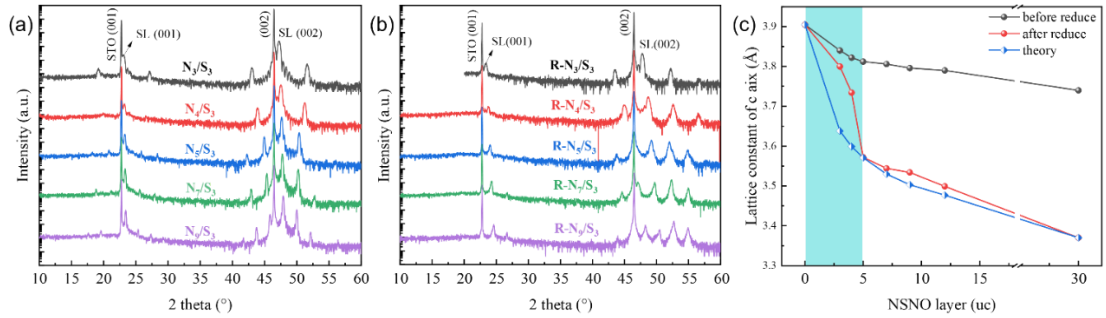

Figure S3. θ-2θ XRD spectra of **(a)** as-grown (N_m/S_3) and **(b)** reduced ($R\text{-}N_m/S_3$) superlattices (SLs) with different thickness of nickelates. **(d)** Out-of-plane c-aixs lattice constant as a function of NSNO thickness for $[(NSNO)_n/STO_3]_{10}$ superlattices before reduction, after reduction and the average lattice constant calculated by the bulk. The sudden decrease from n=4 u.c. to 5 u.c. indicates a structural transition.

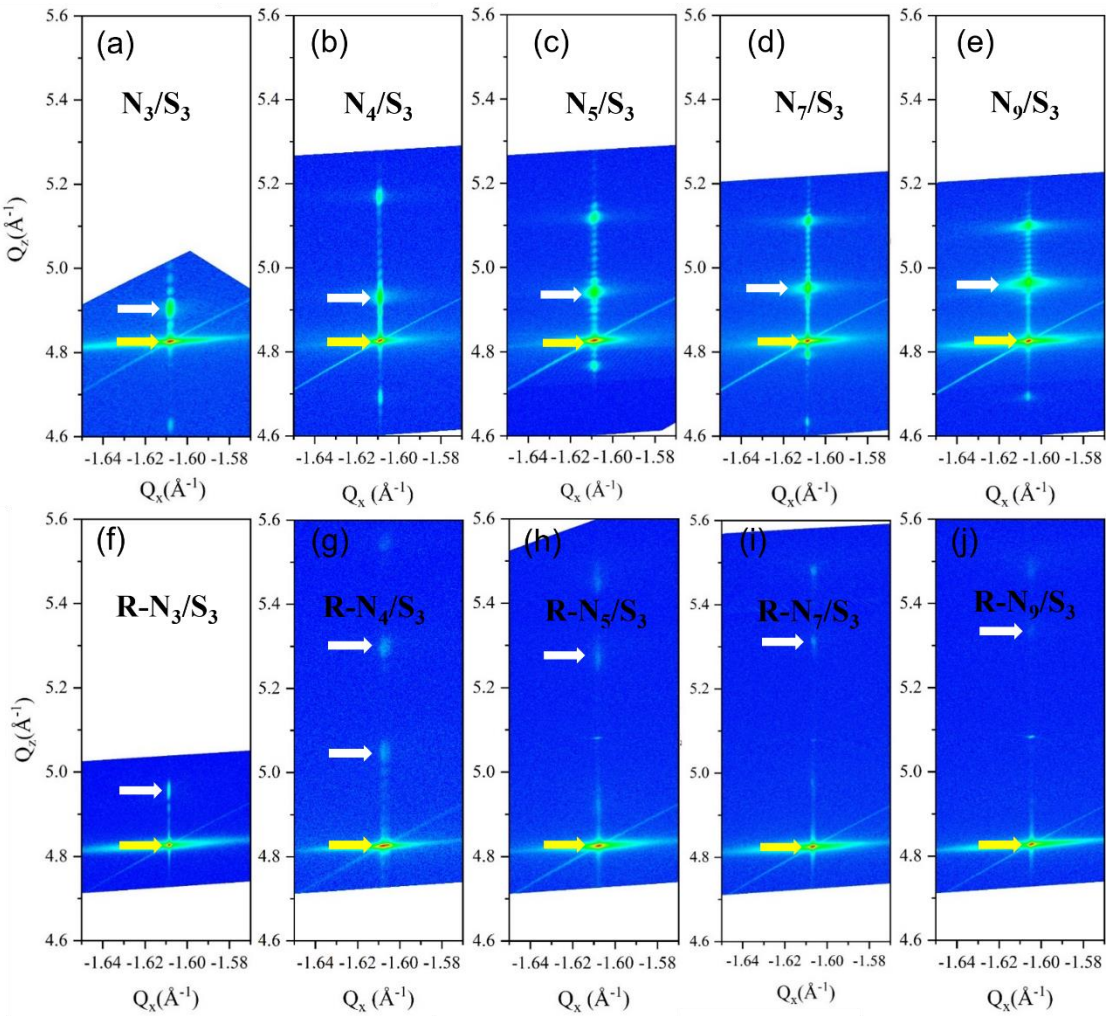

Figure S4. Reciprocal space mapping(RSM) of the (103) peak of $[(NSNO)_n/STO_3]$ superlattices **(a-e)** before reduce and **(f-j)** after reduce. The white and yellow arrows indicate superlattices and $SrTiO_3$ substrate peaks, respectively.

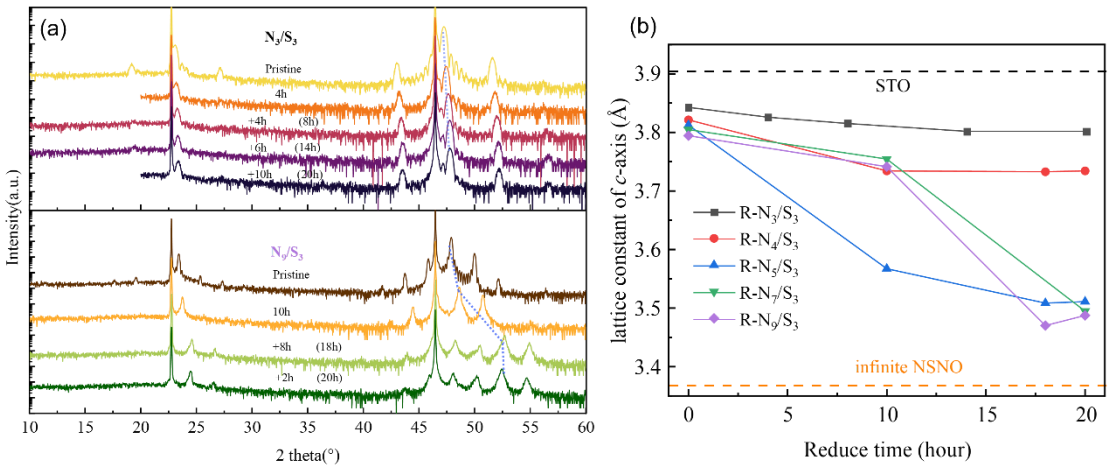

Figure S5. **(a)** Changes of XRD patterns of different superlattices with reduction time (from top to bottom). The reduction process is continuous. **(b)** Out-of-plane c-axis lattice constant as a function of reduce time for $[(NSNO)_n/STO_3]_{10}$ superlattices. The black and orange dashed horizontal lines represent the c-axis lattice constants of STO bulk and infinite-nickelates NSNO, respectively.

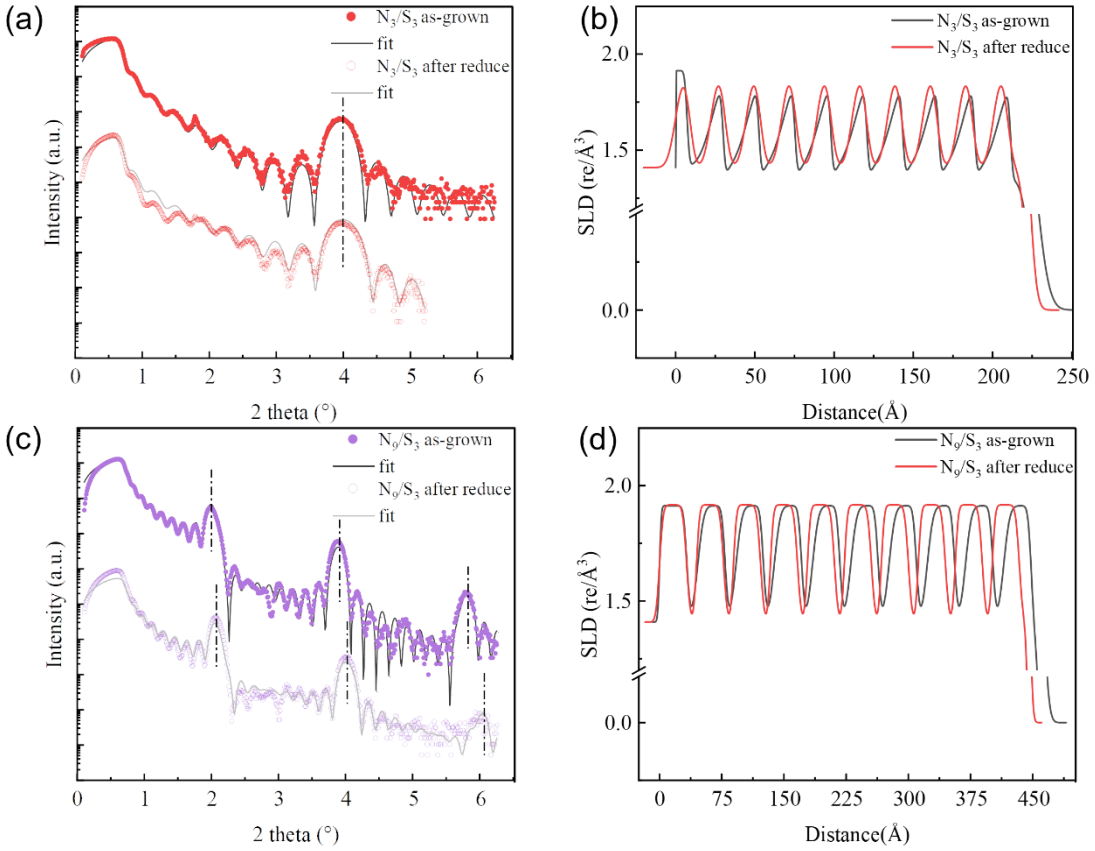

Figure S6. Measured X-ray Reflectivity (XRR) and fit of as-grown and after reduce of (a) N_3/S_3 and (c) N_9/S_3 superlattices. The superlattice peaks are marked with dotted lines. X-ray SLD profiles obtained from the XRR fits for (b) N_3/S_3 and (d) N_9/S_3 superlattices as-grown (dark line) and after reduce (red line).

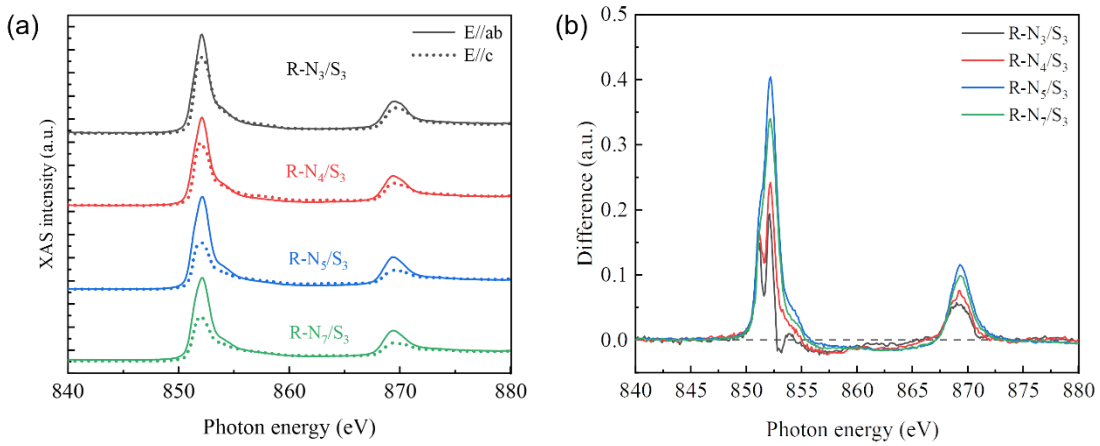

Figure S7. **(a)** Polarization dependent X-ray absorption spectroscopy(XAS) of Ni $L_{2,3}$-edges for superlattices obtained by calcium hydride reduction. **(b)** The X-ray linear dichroism (XLD) defined by $I_{XLD} = I_{E//ab} - I_{E//c}$.

Note 2: Some additional information about R-N_n/S_2

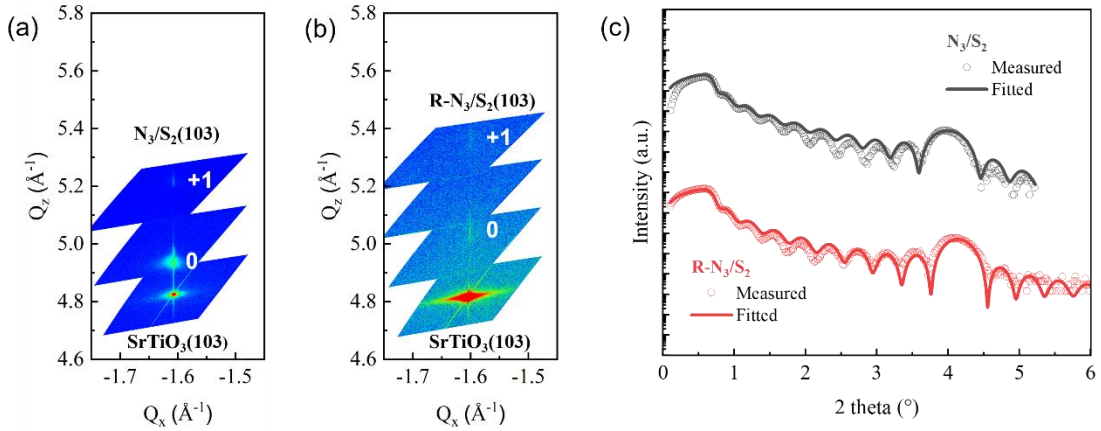

Figure S8. Reciprocal space mapping(RSM) of N_3/S_2 **(a)** and R-N_3/S_2 (103) peaks **(b)**. **(c)** Measured X-ray Reflectivity (XRR) and fitted of N_3/S_2 and R-N_3/S_2 superlattices marked with hollow points and solid lines, respectively.

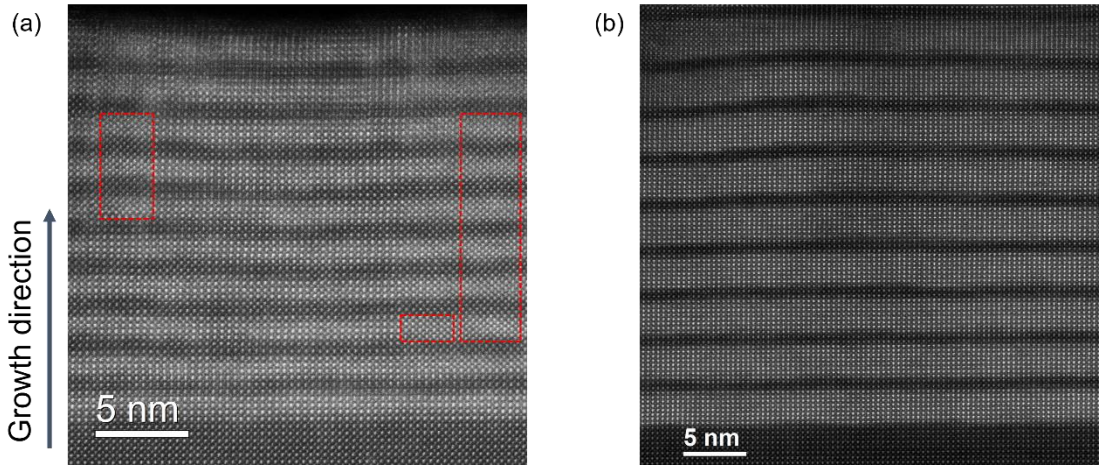

Figure S9. Overview HAADF images of **(a)** R-N_3/S_2 and **(b)** R-N_8/S_2 superlattices, Ruddlesden–Popper (RP) defects in **(a)** are framed by dashed lines.

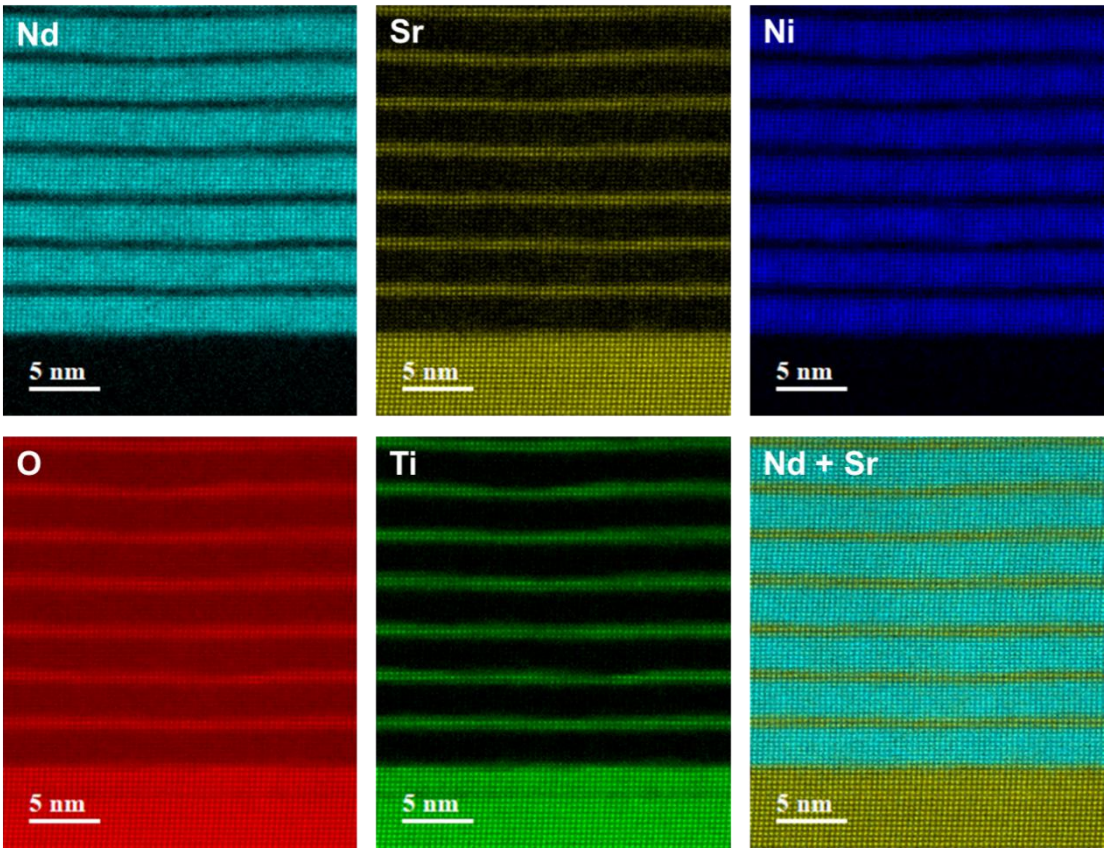

Figure S10. STEM-EELS mappings of R-N_8/S_2. The interface of the superlattice is clearly visible, with no interfacial diffusion and uniform distribution of elements, indicating the high quality of the superlattice.

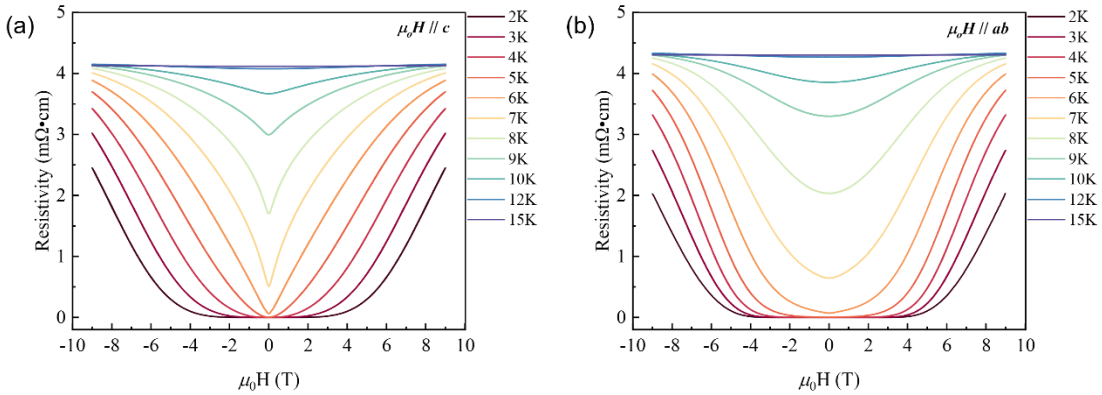

Figure S11. Measured magnetic dependence resistivity under different temperatures from 0 to 9 T for **(a)** $\mu_0 H$ || c and **(b)** $\mu_0 H$ || ab.

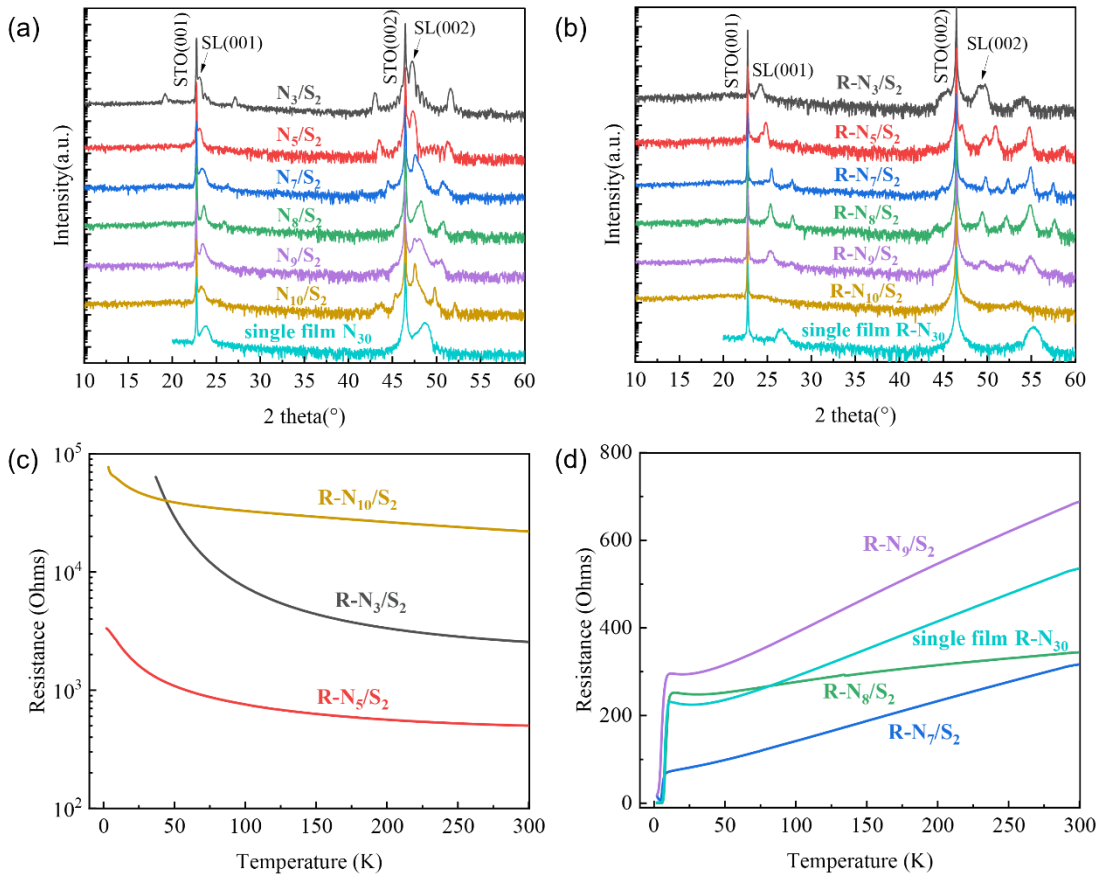

Figure S12. θ-2θ XRD spectra of **(a)** as-grown (N_n/S_2) and **(b)** reduced ($R\text{-}N_n/S_2$) superlattices (SLs) with different thickness of nickelates. As $n > 9$, $R\text{-}N_n/S_2$ is hard to obtain a pure infinite-layer structure. Temperature-dependent resistance R(T) of R- Nn/S2 , (c)when $n \leq 5$ and $n > 9$, the $R\text{-}N_m/S_2$ superlattices exhibit insulating behavior, **(d)** as $5 < n \leq 9$, the $R\text{-}N_n/S_2$ superlattices are superconducting. A single film of 30 u.c. $Nd_{0.8}Sr_{0.2}NiO_{2.3}$ with the same thickness of $SrTiO_3$ capping layers is also included in the **(a)**, **(b)** and **(c)** as comparison data (light blue lines).

Reference

1 Preziosi, D., Sander, A., Barthélémy, A. & Bibes, M. Reproducibility and off-stoichiometry issues in nickelate thin films grown by pulsed laser deposition. *AIP Advances* **7**, 015210 (2017). https://doi.org:10.1063/1.4975307

2 Shi, R. A. *et al.* Scanning SQUID study of ferromagnetism and superconductivity in infinite-layer nickelates. *Physical Review Materials* **8**, 024802 (2024). https://doi.org:10.1103/PhysRevMaterials.8.024802

3 Samal, D. *et al.* Experimental evidence for oxygen sublattice control in polar infinite layer $SrCuO_2$. *Physical Review Letters* **111**, 096102 (2013). https://doi.org:10.1103/PhysRevLett.111.096102

4 Liao, Z. L. *et al.* Large orbital polarization in nickelate-cuprate heterostructures by dimensional control of oxygen coordination. *Nature Communications* **10**, 589 (2019). https://doi.org:10.1038/s41467-019-08472-y

5 Li, S. *et al.* Strong Ferromagnetism Achieved via Breathing Lattices in Atomically Thin Cobaltites. *Advanced Materials* **33**, 2001324 (2020). https://doi.org:10.1002/adma.202001324

6 Li, Z. *et al.* Infinite-layer/perovskite oxide heterostructure-induced high-spin states in $SrCuO_2/SrRuO_3$ bilayer films. *Mater Horiz* **8**, 3468-3476 (2021). https://doi.org:10.1039/d1mh01385h

7 Olafsen, A., Fjellvåg, H. & Hauback, B. C. Crystal Structure and Properties of $Nd_4Co_3O_{10+\delta}$ and $Nd_4Ni_3O_{10-\delta}$. *Journal of Solid State Chemistry* **151**, 46-55 (2000). https://doi.org:10.1006/jssc.2000.8620

8 Lee, K. *et al.* Aspects of the synthesis of thin film superconducting infinite-layer nickelates. *APL Materials* **8**, 041107 (2020). https://doi.org:10.1063/5.0005103

9 Ferenc Segedin, D. *et al.* Limits to the strain engineering of layered square-planar nickelate thin films. *Nat Commun* **14**, 1468 (2023). https://doi.org:10.1038/s41467-023-37117-4

10 Ji, Y. *et al.* Stoichiometry, Orbital Configuration, and Metal-to-Insulator Transition in $Nd_{0.8}Sr_{0.2}NiO_3$ Films. *ACS Appl Mater Interfaces* **15**, 11353-11359 (2023). https://doi.org:10.1021/acsami.2c22387

11 Li, Y. *et al.* Impact of Cation Stoichiometry on the Crystalline Structure and Superconductivity in Nickelates. *Frontiers in Physics* **9**, 719534 (2021). https://doi.org:10.3389/fphy.2021.719534

12 Lee, K. *et al.* Linear-in-temperature resistivity for optimally superconducting $(Nd,Sr)NiO_2$. *Nature* **619**, 288-292 (2023). https://doi.org:10.1038/s41586-023-06129-x

13 Gutiérrez-Llorente, A. *et al.* Toward Reliable Synthesis of Superconducting Infinite Layer Nickelate Thin Films by Topochemical Reduction. *Advanced Science* **11**, 2309092 (2024). https://doi.org:10.1002/advs.202309092